

# Non-local correlations in the orbital selective Mott phase of a one dimensional multi-orbital Hubbard model

S. Li,<sup>1</sup> N. Kaushal,<sup>1</sup> Y. Wang,<sup>1</sup> Y. Tang,<sup>2</sup> G. Alvarez,<sup>3,4</sup> A. Nocera,<sup>3,4</sup> T. A. Maier,<sup>3,4</sup> E. Dagotto,<sup>1,5</sup> and S. Johnston<sup>1</sup>

<sup>1</sup>*Department of Physics and Astronomy, The University of Tennessee, Knoxville, Tennessee 37996, USA*

<sup>2</sup>*Department of Physics, Virginia Tech, Blacksburg, Virginia 24061, USA*

<sup>3</sup>*Center for Nanophase Materials Sciences, Oak Ridge National Laboratory, Oak Ridge, Tennessee 37831, USA*

<sup>4</sup>*Computer Science and Mathematics Division, Oak Ridge National Laboratory, Oak Ridge, Tennessee 37831, USA.*

<sup>5</sup>*Materials Science and Technology Division, Oak Ridge National Laboratory, Oak Ridge, Tennessee 37831, USA*

(Dated: August 19, 2016)

We study non-local correlations in a three-orbital Hubbard model defined on an extended one-dimensional chain using determinant quantum Monte Carlo and density matrix renormalization group methods. We focus on a parameter regime with robust Hund's coupling, which produces an orbital selective Mott phase (OSMP) at intermediate values of the Hubbard  $U$ , as well as an orbitally ordered ferromagnetic insulating state at stronger coupling. An examination of the orbital- and spin-correlation functions indicates that the orbital ordering occurs before the onset of magnetic correlations in this parameter regime as a function of temperature. In the OSMP, we find that the self-energy for the itinerant electrons is momentum dependent, indicating a degree of non-local correlations while the localized electrons have largely momentum independent self-energies. These non-local correlations also produce relative shifts of the hole-like and electron-like bands within our model. The overall momentum dependence of these quantities is strongly suppressed in the orbitally-ordered insulating phase.

PACS numbers:

## I. INTRODUCTION

In recent years the scientific community renewed its interest in understanding the properties of multi-orbital Hubbard models, and this has been intensified by the discovery of the iron-based superconductors.<sup>1-4</sup> On a theoretical front, this is a challenging problem due to a lack of non-perturbative methods for treating multi-orbital Hubbard models at intermediate or strong couplings and on extended systems. Nevertheless, considerable progress has been made using mean-field-based approaches,<sup>4-16</sup> resulting in new concepts such as that of a Hund's metal<sup>7,10,17,18</sup> and the orbital-selective Mott phase (OSMP).<sup>10,19</sup> These concepts are central to our understanding the paradoxical appearance of both localized and itinerant characteristics in many multi-orbital systems<sup>20,21</sup> and bad metallic behavior in the presence of sizable electronic correlations.<sup>21</sup>

The most widely used numerical approach in this context is single-site multi-orbital dynamical mean-field theory (DMFT).<sup>4,22,23</sup> Generally speaking, DMFT maps the full lattice problem onto an impurity problem embedded in an effective medium, which approximates the electron dynamics on a larger length scale as a local renormalization.<sup>23</sup> While this technique has had considerable success in addressing many aspects of the OSMP and other physics related to the multi-orbital problem,<sup>8,9,12-14,24-28</sup> it is unable to capture spatial fluctuations and non-local correlations encoded in the  $k$ -dependent self-energy  $\Sigma(\mathbf{k}, \omega)$ . This is a potential short coming as non-local correlations are known to have an impact in the case of the single-band Hubbard model.<sup>29,30</sup> It is therefore important to assess the importance of such

non-local effects on multi-orbital properties such as the OSMP.

To date, most non-perturbative studies have used cluster DMFT or the dynamical cluster approximation (DCA);<sup>16,31-35</sup> however, these techniques are typically limited to a handful of sites when multiple orbitals are included in the basis. This is due to technical issues related to each choice in impurity solver, such as the Fermion sign problem in the case of quantum Monte Carlo or the exponential growth of the Hilbert space in the case of exact diagonalization. As a result, these studies have only addressed short-range spatial fluctuations. One study of the OSMP has been carried out on a larger two-dimensional cluster using determinant quantum Monte Carlo (DQMC). In that case, however, the OSMP was imposed by the model by assuming that electrons in a subset of orbitals were localized as Ising spins.<sup>36</sup> In light of these limitations it is desirable to find situations where multi-orbital physics can be modeled on extended clusters that support long-range spatial fluctuations and where the properties under study emerge from the underlying many-body physics of the model.

In this regard, one dimensional (1D) models are quite promising. For example, two recent density matrix renormalization group (DMRG) studies have been carried out for an effective 1D three-orbital model representative of the iron-based superconductors.<sup>37,38</sup> More recently, it was demonstrated that DQMC simulations for a simplified version of the same model can also be carried out to low temperatures due to a surprisingly mild Fermion sign problem.<sup>39</sup> These observations open the doorway to non-perturbative studies of this model on extended clusters, thus granting access to the

momentum-resolved self-energies and non-local correlations. 1D studies along these lines are also directly relevant for the recently-discovered quasi-1D selenide  $\text{Ba}_{1-x}\text{K}_x\text{Fe}_2\text{Se}_3$ .<sup>40–45</sup> In this context, it is important to note that DMFT becomes more accurate in higher dimensions and therefore one expects its ability to describe multi-orbital Mott physics in 1D to be diminished.

Motivated by these considerations, we examine the properties of a three-orbital Hubbard Hamiltonian on an extended 1D cluster using DQMC and DMRG, with a particular focus on its  $k$ -resolved self-energies and spectral properties. We thus gain explicit access to non-local correlations occurring on longer length scales than those addressed in previous non-perturbative studies. In general, we find that the OSMF leads to a mixture of localized and itinerant bands, where the former are characterized by a localized (momentum-independent) self-energy while the latter exhibits significant non-local (momentum-dependent) correlations. This leads to a band-dependent shift of the underlying band structures. We also identify an insulating state driven by orbital ordering in a region of parameter space previously associated with an OSMF.<sup>37,38</sup>

## II. METHODS

### A. Model Hamiltonian

We study a simplified three-orbital model defined on a 1D chain as introduced in Ref. 37. This model displays a rich variety of phases including block ferromagnetism, antiferromagnetism, Mott insulating phases, metallic and band insulating phases, and several distinct OSMFs.<sup>37–39</sup> The Hamiltonian is  $H = H_0 + H_{\text{int}}$ , where

$$H_0 = - \sum_{\substack{\langle i,j \rangle \\ \sigma, \gamma, \gamma'}} t_{\gamma\gamma'} c_{i,\gamma,\sigma}^\dagger c_{j,\gamma',\sigma} + \sum_{i,\sigma,\gamma} (\Delta_\gamma - \mu) \hat{n}_{i,\gamma,\sigma} \quad (1)$$

contains the non-interacting terms of  $H$ , and

$$H_{\text{int}} = U \sum_{i,\gamma} \hat{n}_{i,\gamma,\uparrow} \hat{n}_{i,\gamma,\downarrow} + \left( U' - \frac{J}{2} \right) \sum_{\substack{i,\sigma,\sigma' \\ \gamma < \gamma'}} \hat{n}_{i,\gamma,\sigma} \hat{n}_{i,\gamma,\sigma'} \\ + J \sum_{i,\gamma < \gamma'} S_{i,\gamma}^z S_{i,\gamma'}^z$$

contains the on-site Hubbard and Hund's interaction terms. Here,  $\langle \dots \rangle$  denotes a sum over nearest-neighbors,  $c_{i,\gamma,\sigma}^\dagger$  ( $c_{i,\gamma,\sigma}$ ) creates (annihilates) a spin  $\sigma$  electron in orbital  $\gamma = 1, 2, 3$  on site  $i$ ,  $\Delta_\gamma$  are the on-site energies for each orbital,  $S_{i,\gamma}^z$  is the z-component of the spin operator  $\mathbf{S}_{i,\gamma}$ , and  $\hat{n}_{i,\gamma,\sigma} = c_{i,\gamma,\sigma}^\dagger c_{i,\gamma,\sigma}$  is the particle number operator. The pair-hopping and spin-flip terms of the interaction have been neglected in order to manage the sign problem in the DQMC calculations.

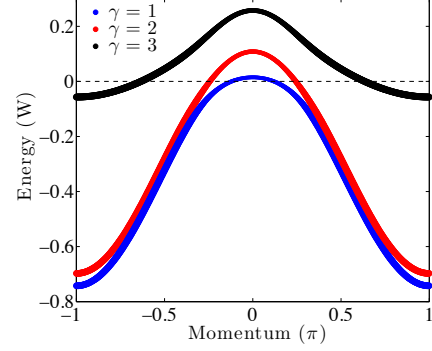


FIG. 1: (color online) A fat band plot of the non-interacting band structure at a total filling of  $\langle \hat{n} \rangle = 4$ , where the thickness of the lines indicates the majority orbital content of the band. The top most band has the narrowest bandwidth and is primarily of orbital 3 character. The lower two bands disperse over a much larger energy range and are primarily composed of orbitals 1 and 2, respectively.

Following Ref. 37, we set  $t_{11} = t_{22} = -0.5$ ,  $t_{33} = -0.15$ ,  $t_{13} = t_{23} = 0.1$ ,  $t_{12} = 0$ ,  $\Delta_1 = -0.1$ ,  $\Delta_2 = 0$ , and  $\Delta_3 = 0.8$  in units of eV while the chemical potential  $\mu$  is adjusted to obtain the desired filling. These parameters produce a non-interacting band structure analogous to the iron-based superconductors, with two hole-like bands centered at  $k = 0$  and an electron-like band centered at  $k = \pi/a$ , as shown in Fig. 1. Due to the weak inter-orbital hopping, each of the bands is primarily derived from a single orbital, as indicated by the line thickness and colors in Fig. 1. One can therefore (loosely) regard the orbital character as an indicator of the band in this model. For example, the top most band is primarily composed of orbital  $\gamma = 3$ . The total bandwidth of the non-interacting model is  $W = 4.9|t_{11}| = 2.45$  eV. This will serve as our unit of energy. We further set  $a = 1$  as our unit of length. The interaction parameters are fixed to  $U' = U - 2J$ ,  $J = U/4$ , while  $U$  is varied. This parameter regime results in a robust OSMF for intermediate values of  $U$ , which is our focus here.

### B. DQMC and DMRG Calculations

The model is studied using non-perturbative DQMC and DMRG methods. The details of these techniques can be found in Refs. 46–48 (DQMC) and Refs. 49 and 50 (DMRG). These approaches are complementary to one another; DMRG works in the canonical ensemble and provides access to the ground state properties of the system while DQMC works in the grand canonical ensemble and provides access to finite temperatures and fluctuations in particle number. Both methods are capable of treating large cluster sizes such that non-local correlations can be captured without approximation for the specified Hamiltonian.

The primary drawback to DQMC is the Fermion sign problem,<sup>51,52</sup> which typically limits the range of accessible temperatures for many models. Indeed, when the spin-flip and pair hopping terms of the Hund's interaction are included in the Hamiltonian, we find that the model has a prohibitive sign problem. But when these terms are neglected the corresponding sign problem becomes very mild,<sup>39</sup> even in comparison to similar simplified multi-orbital models in 2D.<sup>48,53</sup> Given that these terms do not qualitatively affect the phase diagram<sup>39</sup> for the current model, we have neglected them here. This has allowed us to study clusters of up to  $L = 24$  sites in length ( $3L$  orbitals in total) down to temperatures as low as  $\beta = 74/W$ .<sup>39</sup> At this low of a temperature we begin to see the onset of magnetic correlations in our cluster, however, as we will show, the OSMF forms at a much higher temperature. Since the latter phase is our focus here, we primarily show DQMC results for  $\beta \leq 19.6/W$  throughout. In all cases shown here, the average value of the Fermion sign is greater than  $0.87 \pm 0.01$ . Unless otherwise stated, all of our DQMC results were obtained on an  $L = 24$  site cluster with periodic boundary conditions and for an average filling of  $\langle n \rangle = 4$  electrons, which corresponds to  $2/3$  filling.

DQMC provides direct access to various quantities defined in the imaginary time  $\tau$  or Matsubara frequency  $i\omega_n$  axes. In Sec. IIID we will examine the spectral properties of our model, which requires an analytic continuation to the real frequency axis. This was accomplished using the method of Maximum Entropy,<sup>54</sup> as implemented in Ref. 55.

Our DMRG results were obtained on variable length chains with open boundary conditions. The chemical potential term in Eq. (1) is dropped for these calculations. In all of the DMRG calculations the truncation tolerance is between  $10^{-5} - 10^{-7}$ . We performed three to five full sweeps of finite DMRG algorithm and used 300 states for calculating both the ground state and the spectral function. Once the ground state is obtained using the standard DMRG algorithm, we computed the spectral function using the correction vector targeting in Krylov space<sup>56,57</sup>, with an broadening of  $\eta = 0.001$  eV.

### III. RESULTS

#### A. Self-energies in the OSMF

We begin by examining some of the standard metrics for the formation of an OSMF, namely the average filling per orbital and the quasiparticle residue  $Z_\gamma(k, i\omega_n)$ . DQMC results for  $\langle n \rangle = 4$  and  $U/W = 0.8$  are summarized in Fig. 2. The temperature dependence of the individual orbital occupations  $\langle n_\gamma \rangle$ , plotted in Fig. 2a, has the standard indications of the formation of an OSMF: At high temperature (small  $\beta$ ) we see noninteger fillings for all three orbitals. As the temperature is lowered (large  $\beta$ ), however, orbitals one and two smoothly approach fill-

ings of  $\sim 1.53$  and  $\sim 1.47$ , respectively, while orbital three locks into an integer value of exactly 1. In some studies these values for the average occupation are often taken as an indication of an OSMF,<sup>37,38</sup> where orbital three has undergone a transition to a Mott insulating state while orbitals one and two host itinerant electrons. However, as we will show, this is not always the case. For  $U/W = 0.8$  the two fractionally filled orbitals are in fact itinerant, but for larger values of  $U/W$  these same orbitals retain a fractional filling but are driven into an insulating state by the onset of orbital ordering in these two orbitals.

The mixed itinerant/localized nature of the OSMF at  $U/W = 0.8$  is reflected in the momentum dependence of quasi-particle residue  $Z_\gamma(k, i\pi/\beta)$  and the orbitally resolved normalized self-energies  $R(k) = \text{Im}\Sigma_\gamma(k, i\pi/\beta)/\text{Im}\Sigma_\gamma(0, i\pi/\beta)$ , plotted in Figs. 2c and 2d, respectively, for  $\omega_n = \pi/\beta$ . The self-energy is extracted from the dressed Green's function using Dyson's equation

$$\hat{G}^{-1}(k, i\omega_n) = \hat{G}_0^{-1}(k, i\omega_n) - \hat{\Sigma}(k, i\omega_n), \quad (2)$$

where the  $\hat{G}$  notation denotes a matrix in orbital space,  $\hat{G}_0(k, i\omega_n) = [i\omega_n \hat{I} - \hat{H}_0(k)]^{-1}$  is the non-interacting Green's function, and  $\hat{H}_0(k)$  is the Fourier transform of the non-interacting Hamiltonian defined in orbital space. The quasi-particle residue is obtained from the diagonal part of the self-energy using the identity

$$\hat{Z}(k, i\pi/\beta) = \left( \hat{I} - \frac{\text{Im}\hat{\Sigma}(k, i\pi/\beta)}{\pi/\beta} \right)^{-1}, \quad (3)$$

where  $\hat{I}$  is a  $3 \times 3$  unit matrix.

As can be seen from Fig. 2c, the self-energies for each orbital have a sizable  $k$ -dependence at this temperature. (In this case we have normalized the self-energy by its value at  $k = 0$  in order to highlight the overall momentum dependence. The magnitude of  $\text{Im}\Sigma_\gamma(0, i\pi/\beta)$  is given in the figure caption.) In the case of orbitals one and two, the magnitude of the self-energy varies by nearly 50% throughout the Brillouin zone. In contrast, the momentum dependence of  $\Sigma_3(k, i\pi/\beta)$  for orbital three is much weaker, varying by only 5-10% and reflecting the localized nature of the carriers in these orbitals. Similarly, the quasi-particle residue for the orbital three is essentially momentum independent, while it increases for the two itinerant orbitals as  $k$  tracks towards the zone boundary. The  $k$  dependence at the remaining Matsubara frequencies accessible to our simulations (not shown) exhibits a similar trend, with orbitals one and two having a strong  $k$ -dependence while orbital three is nearly momentum independent at each  $\omega_n$ .

The momentum dependence shown in Fig. 2 indicates that the local self-energy approximation introduced by DMFT may miss quantitative aspects of the electronic correlations in the OSMF with mixed itinerant and local characteristics. It should be noted that our results

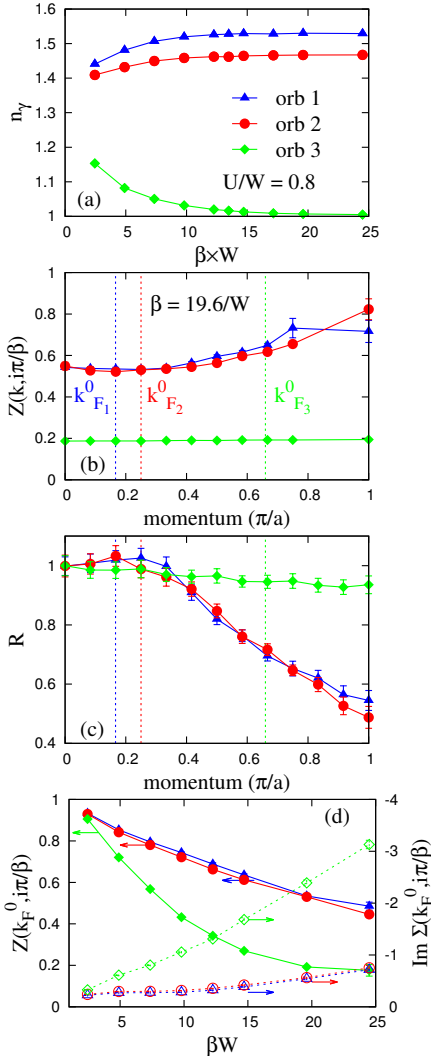


FIG. 2: (color online) Orbitaly resolved electronic properties for  $U/W = 0.8$  ( $W = 2.45$  eV) at different temperatures. (a) The temperature dependence of orbital occupations. (b) The orbital resolved quasiparticle residue  $Z_\gamma(k, i\pi/\beta)$  at an inverse temperature  $\beta = 19.6/W$ . (c) The normalized electron self energies  $\text{Im}\Sigma_\gamma(k, i\pi/\beta)$  at  $\omega_n = \pi/\beta$  as a function of momentum. Each curve is normalized by its  $k = 0$  value to highlight the overall momentum dependence. The scale is determined by  $\text{Im}\Sigma_\gamma(0, i\pi/\beta) = -0.53, -0.57, \text{ and } -2.53$  for  $\gamma = 1, 2, 3$ , respectively, and in units of the bandwidth  $W$ . The blue, red, and green dash lines in (b) and (c) correspond to the bare Fermi momentum of the non-interacting bands. Panel (d) shows orbitaly resolved quasiparticle residues  $Z_\gamma(k_F^0, i\pi/\beta)$  and self energies  $\text{Im}\Sigma_\gamma(k_F^0, i\pi/\beta)$  at Fermi momentum as a function of temperature. In each panel, error bars smaller than the marker size have been suppressed for clarity.

have been obtained in 1D, which is the worst case situation for DMFT.<sup>58</sup> It is expected that the local approximation will perform better in higher dimensions, since DMFT becomes exact in the limit of infinite dimensions; however, it is unclear how well the method will capture similar non-local correlations in two dimensions relevant

for the Fe-based superconductors. A recent study<sup>16</sup> has argued that the local approximation is quite accurate for parameters relevant to the iron-based superconductors, however, it remains to be seen if this will remain true for all parameter regimes or when longer range fluctuations are included. Our results further highlight the need for the continued development of numerical methods capable of handling the strong Hubbard and Hund's interactions in intermediate dimensions and on extended clusters.

Figure 2d examines the temperature dependence of  $Z(k_F^0, i\pi/\beta)$  and  $\text{Im}\Sigma(k_F^0, i\pi/\beta)$  at the Fermi momenta  $k_F^0$  of the non-interacting system. (These are indicated by the dashed lines in 2b and 2c.) Here, we find indications of anomalous behavior for the itinerant electrons, where the quasiparticle residues of all three orbitals decrease with temperature. This is accompanied by an increase in  $\text{Im}\Sigma(k_F, i\pi/\beta)$  as  $T$  is lowered. This is perhaps expected for orbital three, as  $Z$  ( $\text{Im}\Sigma$ ) for the localized orbitals should decrease (increase) as this orbital becomes more localized. For the itinerant orbitals, however, one would naively expect the self-energy to decrease as temperature is lowered, which is opposite to what is observed. We believe that this is due to the Hund's interaction between the itinerant electrons and the localized spins on orbital three. At this temperature we find no evidence of a magnetic ordering in our model,<sup>39</sup> despite the fact that a local moment has clearly formed in the OSMF. This means that the orientation of the local moment is random and fluctuating at these temperatures. This produces a fluctuating potential acting on the itinerant electrons via the Hund's coupling, thus generating a residual scattering mechanism at low temperatures that reduces the quasiparticle residue and increases the self-energy.

## B. Momentum and Temperature Dependence of the Spectral Weight

Next, we turn to the momentum dependence of the spectral weight for the three orbitals in the vicinity of the Fermi level. This can be estimated directly from the imaginary time Green's function, where the spectral weight at momentum  $k$  is proportional to  $\beta G(k, \tau = \beta/2)$ .<sup>59</sup> Using this relationship we do not have to perform the extra step of analytically continuing the data to the real frequency axis.

Figures 3a-3c summarize  $\beta G(k, \beta/2)$  for  $U/W = 0.1$ ,  $U/W = 0.8$ , and  $U/W = 2$ , respectively. The results in the weak coupling limit ( $U/W = 0.1$ , Fig. 3a) are consistent with that of a fully itinerant system: all three orbitals have a maximal spectral weight at a momentum point very close to the Fermi momenta of the non-interacting system (indicated by the dashed lines). This is exactly the behavior one expects for a well-defined quasi-particle band dispersing through  $E_F$ , where the peak in the spectral weight occurs at  $k_F$ . The proximity of the peaks in  $\beta G(k, \beta/2)$  to the non-interacting values of  $k_F$  indicates that the Fermi surface is only weakly

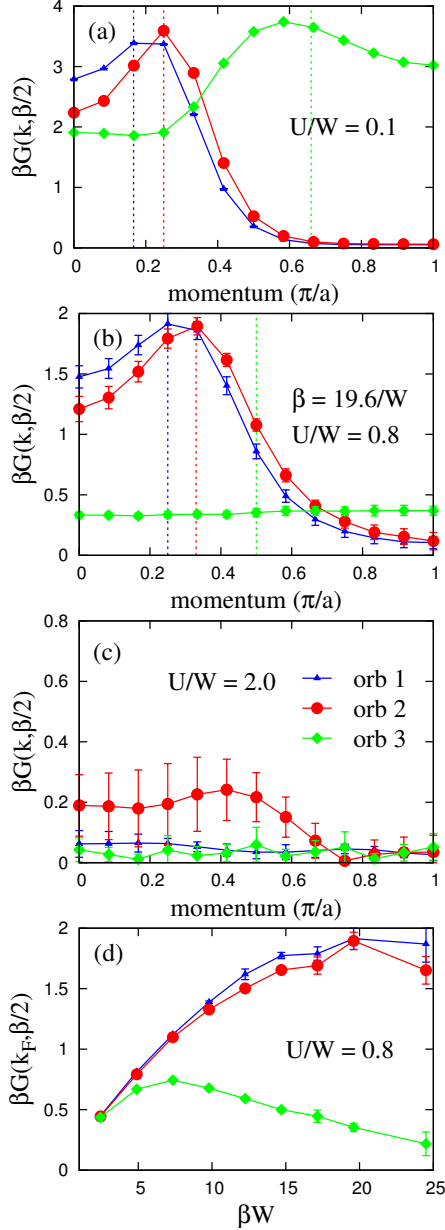


FIG. 3: (color online) The momentum dependence of Green functions  $G(k, \tau = \beta/2)$  for a)  $U/W = 0.1$ , b)  $0.8$ , and c)  $2.0$ . The inverse temperature in all three cases is  $\beta = 19.6/W$ . The blue, red, and green dash lines in each panel indicate the Fermi momentum of the three non-interacting bands. (d)  $G(k_F, \tau = \beta/2)$  as a function of inverse temperatures  $\beta$  for the OSMP  $U/W = 0.8$ . Error bars smaller than the marker size have been suppressed for clarity.

shifted for this value of the interaction parameters. However, as we will show in Sec. III C, these shifts are band dependent.

In the intermediate coupling regime ( $U/W = 0.8$ , Fig. 3b), where the OSMP has formed, we again see both localized and itinerant characteristics. The spectral weight of the localized orbital is small and independent of mo-

mentum, as expected for the formation of a localized Mott state. Conversely, the spectral weight of the remaining orbitals still exhibits a momentum dependence characteristic of dispersive bands. Despite this, the total spectral weight is decreased, indicating that spectral weight has been transferred to higher binding energies by the Hubbard and Hund's interactions. This is also reflected in the position of the maximum spectral weight, which has shifted to a slightly larger  $k$  value due to a renormalization of the Fermi surface by the interactions. We also observe that the spectral weight at the zone boundary increases relative to the zone center, consistent with a flattening of the bands and a broadening of the spectral function with increasing  $U$ . (This will be confirmed shortly when we examine the spectral functions directly.) A similar transfer of spectral weight was observed in a two-dimensional cluster DMFT study.<sup>35</sup>

The temperature evolution of spectral weight  $\beta G(k_F, \beta/2)$  at the Fermi momentum for the OSMP ( $U/W = 0.8$ ) is shown in Figure 3d. In a metallic system one generally expects the spectral weight at the Fermi level to increase as the temperature is decreased. Initially, this is what is observed for all three orbitals, however, the spectral weight for orbital three reaches a maximum around  $\beta = 7.5/W$  before decreasing as the temperature is lowered further and the OSMP gap forms on this orbital. Conversely, the spectral weight of the itinerant orbitals continues to rise until saturating at  $\beta/W \approx 15$ . This saturation is again due to the presence of a residual scattering channel, which we associate with the fluctuating localized spins present on the localized orbital three.

The  $U/W = 0.8$  results confirm the mixed itinerant/local character of the model at intermediate coupling. When the value of  $U$  is further increased, we find that all three bands become localized while maintaining partial occupancies for each band. To demonstrate this, Fig. 3c shows results for  $U/W = 2$ . In this case, the orbital occupations for the three orbitals are  $\langle n_1 \rangle = 1.55$ ,  $\langle n_2 \rangle = 1.44$ ,  $\langle n_3 \rangle = 1$ , which are similar to those obtained at  $U/W = 0.8$ . At face value one might therefore conclude that the system is in an OSMP,<sup>37,39</sup> however, an examination of the spectral weight reveals that the system is in fact insulating. As can be seen in Fig. 3c, at  $U/W = 2$  and  $\beta = 19.6/W$ ,  $\beta G(k, \beta/2)$  is nearly momentum independent and the total spectral weight of all three orbitals has significantly decreased (note the change in scale of the y-axis). This behavior is indicative of the formation of a charge gap throughout the Brillouin zone. The ultimate origin of this insulating behavior is the formation of a long-range orbital ordering, as we will show in Sec. III D.

### C. Band-dependent Fermi surface renormalization

It is now well known that *ab initio* band structure calculations based on density functional theory (DFT) do



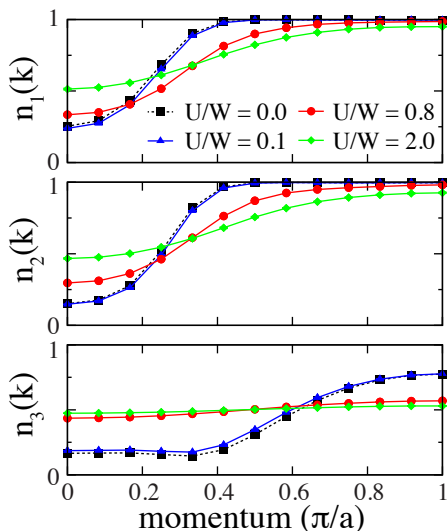


FIG. 4: (color online) The momentum dependence of the number operator  $n_\gamma(k) = \frac{1}{2} \sum_\sigma \langle c_{\mathbf{k},\gamma,\sigma}^\dagger c_{\mathbf{k},\gamma,\sigma} \rangle$  for each band. Results are shown for the non-interacting case  $U = 0$  (black dashed,  $\square$ ),  $U/W = 0.1$  (blue solid,  $\triangle$ ),  $U/W = 0.8$  (red solid  $\circ$ ), and  $U/W = 2$  (green solid  $\diamond$ ) and at an inverse temperature of  $\beta = 19.6/W$ .

not describe the electronic structure of the iron based superconductors as measured in ARPES experiments. (For a recent review, see Ref. 4.) Generally speaking, the calculated band structure usually needs to be rescaled by an overall factor, which is attributed to reduction in bandwidth driven by electronic correlations. In addition, the size of the Fermi surfaces is often overestimated by DFT in comparison to measurements. A prominent example of this is LiFeAs,<sup>60</sup> where the inner most hole pocket realized in nature is substantially smaller than the one predicted by DFT<sup>61,62</sup>. In order to correct this, the electron- and hole-bands need to be shifted apart,<sup>4</sup> which requires a momentum-dependent self-energy correction.

We examine this issue within our model in Fig. 4, which plots the expectation value of the orbitally-resolved number operator in momentum space  $n_\gamma(k) = \frac{1}{2} \sum_\sigma \langle c_{\mathbf{k},\gamma,\sigma}^\dagger c_{\mathbf{k},\gamma,\sigma} \rangle$  for various values of the interaction strength. In the non-interacting limit, and in a single-band case, this quantity is equal to the Fermi-Dirac distribution and the location of the leading edge corresponds to  $k_F$ . In a multi-band system the mixing of the orbital character complicates this picture; however, in our model the leading edge still corresponds to  $k_F$  due to the weak hybridization between orbitals. In the weak coupling case ( $U/W = 0.1$ ) we observe a small shift in the position of the leading edge. Within error bars, the curve  $n_1(k)$  and  $n_2(k)$  shift to slightly larger momenta while  $n_3(k)$  shifts towards smaller momenta. This indicates that the size of the Fermi surfaces are increasing and the electron-like and hole-like bands are shifted towards one another by the interactions. This trend continues as  $U/W$  is in-

creased to 0.8; however, in this case the electron-like band is significantly smeared out due to the formation of the OSMP.

We note that the direction of the band shifts is reversed from what is generally required for the two-dimensional iron-based superconductors, where the calculated hole-like Fermi surfaces generally need to be shrunk relative to the electron-like Fermi surfaces. We attribute this to differences in the underlying tight-binding model and differences in dimensionality. In this light, it would be interesting to compare the ARPES observed band structures in the quasi-one-dimensional pnictides against the predictions of our model and DFT calculations.<sup>42</sup> Nevertheless, our results do show that non-local correlations arising from a local interaction can produce relative shifts of the electron-like and hole-like bands in a multi-orbital system.

## D. Spectral Properties

### 1. Intermediate Coupling $U/W = 0.8$

We now examine the spectral properties of the model, beginning with the OSMP. Figure 5a shows the temperature evolution of the total density of states (DOS) at  $U/W = 0.8$ , which is obtained from the trace of the orbital-resolved spectral function  $N(\omega) = \sum_{k,\gamma} -\frac{1}{\pi} \text{Im} \hat{G}_{\gamma\gamma}(k, \omega + i\delta)$ . In the non-interacting limit (the long-dashed (blue) curve), the DOS has a double peak structure, where the lower (upper) peak corresponds to the bands derived from orbitals one and two (orbital three). The overall structure of the DOS in the interacting case is similar at high temperatures, but some spectral weight is transferred to a broad incoherent tail extending to lower energies. As the temperature is decreased, the peak on the occupied side shifts towards the Fermi level and sharpens. At the same time, a small amount of spectral weight is transferred from the vicinity of the Fermi level into this peak. The appearance of this apparent “pseudogap” is a direct consequence of the OSMP forming on orbital three, which is easily confirmed by examining the orbital-resolved DOS  $N_\gamma(\omega) = -\frac{1}{\pi} \sum_k \text{Im} \hat{G}_{\gamma,\gamma}(k, \omega)$  shown in Fig. 5b. As can be clearly seen, orbitals one and two have a finite DOS at  $\omega = 0$ , while orbital three is fully gapped at low-temperature.

We also begin to see the formation of an additional peak near the Fermi level at the lowest temperature we examined ( $\beta = 19.6/W$ ). This feature is more clearly seen in the orbital-resolved DOS (Fig. 5b), where it is found to originate from the itinerant orbitals. This peak is due to a hybridization between the itinerant and localized orbitals, which is observable in the  $k$ -resolved spectral functions (see Fig. 6).

The relevant temperature scale for the formation of the OSMP can be estimated by tracking  $N_3(0)$  as a function of temperature, as shown in Fig. 5c. Here, a continuous

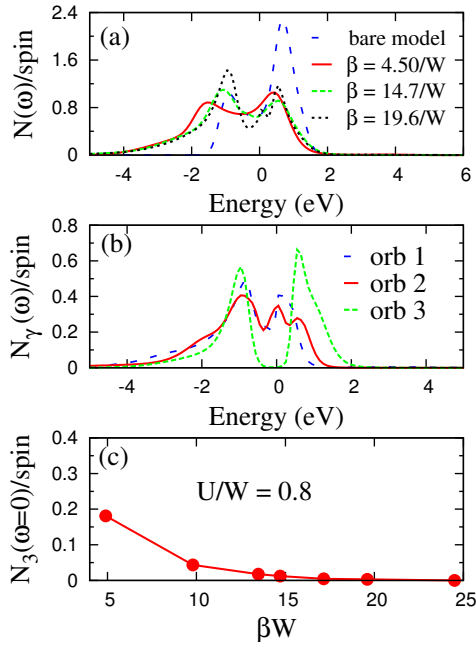


FIG. 5: (color online) (a) The density of states at different temperatures. (b) The orbitaly-resolved density of states for each orbital at an inverse temperature  $\beta = 19.6/W$ . (c) The density of states at the Fermi surface of the orbital 3 as a function of inverse temperatures  $\beta$ . The Coulomb interaction strength is  $U/W = 0.8$  in all three graphs.

suppression of  $N_3(0)$  is observed, with the value reaching zero at  $\beta \approx 20/W$ . The rate at which  $N_3(0)$  decreases also undergoes a distinct change at  $\beta \approx 10/W$ , which coincides with the temperature at which the spectral weight for this orbital at  $k_F$  is largest (see Fig. 3d). We interpret this to mean that the Mott gap on orbital three begins to form at  $\beta W \approx 10$  (on the  $L = 24$  site lattice), growing continuously from zero as the temperature is lowered. In this case, the finite spectral weight between  $\beta W = 10 - 20$  is due to thermal broadening across this gap. Since we have observed similar behavior on smaller clusters with DQMC and at zero temperature using DMRG, we believe that the transition to the OSMF will survive in the thermodynamic limit, however, the gap magnitude has some finite size dependence.

The extended length of our 1D cluster grants us access to the momentum dependence of the spectral function, which is shown in Fig. 6. The top row of Fig. 6 shows the results in the OSMF with  $U/W = 0.8$  and  $\beta = 19.6/W$ , which is the same parameter set used in Fig. 5. The total spectral function  $A(k, \omega) = -\frac{1}{\pi} \text{Tr} [\text{Im} \hat{G}(k, \omega)]$  is shown in Fig. 6a and the orbital-resolved components  $A_\gamma(k, \omega) = -\frac{1}{\pi} \text{Im} \hat{G}_{\gamma\gamma}(k, \omega)$  are shown in Figs. 6b-d, as indicated. The lower row of Fig. 6 shows similar results obtained for  $U/W = 2$  and  $L = 8$ . (In this case a smaller cluster is sufficient due to the non-dispersing nature of the band dispersions.)

The results in the OSMF with  $U/W = 0.8$  reveal local-

ized and itinerant characteristics that are consistent with the spectral weight analysis presented earlier. The itinerant orbitals primarily contribute to dispersing bands that track through the  $E_F$  ( $\omega = 0$ ), while orbital three has split into two relatively dispersionless upper and lower Hubbard bands above and below  $E_F$ . At first glance, these Hubbard bands appear to be sharper than the corresponding Hubbard bands in the single-band Hubbard model; however, an examination of the DOS (Fig. 5b) reveals that they are spread out over an energy interval that is larger than the non-interacting bandwidth of the top most band ( $W_3 \sim 0.3W \sim 0.735$  eV). In addition to the formation of the Hubbard bands for orbital 3, we also observe two additional effects. The first is an expected narrowing of the bandwidth of the itinerant bands. For this parameter set we obtain  $W_1 \sim 1.7$  and  $W_2 \sim 1.65$  eV for orbitals one and two, respectively, which should be compared to the non-interacting values of 1.88 and 1.97 eV. The second is the aforementioned hybridization and level repulsion between the itinerant and localized orbitals. This is manifest in the spectral function as a slight “buckling” of orbital three’s upper Hubbard band near  $k = 0$ , and the tracking orbital one’s spectral weight along  $E_F$  near  $k = \pm\pi/2a$ . It is this trailing intensity that forms the peak observed in the DOS just above the Fermi level at low temperatures.

## 2. Strong Coupling $U/W = 2$

The spectral properties of the model are very different when the Hubbard interaction is increased to  $U/W = 2$ . In this case, the total spectral function (Fig. 6e) and its orbitaly-resolved components (Fig. 6f-h) all split into relatively flat Hubbard-like bands above and below  $E_F$ . (In the case of orbital three, the lower band below  $E_F$  has been pushed outside of the energy range shown in the figure.) For this value of the interaction strength there is no spectral weight at the Fermi level, and the system is insulating even though orbitals one and two have on average 1.55 and 1.44 electrons/orbital, respectively. (These values are obtained both from the measured equal time orbital occupancies, and from integrating the total spectral weight above and below  $E_F$ .)

The imaginary axis spectral weight analysis (Fig. 3c) and the spectral function analysis (Fig. 6) both indicate that for  $U/W = 2$  the model is an insulator. The origin of this behavior is the combined action of the Hund’s coupling and the onset of an orbital ordering of the itinerant orbitals. All indications show that orbital three has already undergone an orbital selective Mott phase transition (OSMT) when  $U/W = 2$ . This has the effect of localizing one electron per site within this subset of orbitals while leaving three additional electrons to be distributed among the remaining two itinerant orbitals. A sizable Hund’s coupling will decouple the individual orbitals when the crystal field splittings are smaller than the bandwidth of the material.<sup>21</sup> This is precisely the sit-

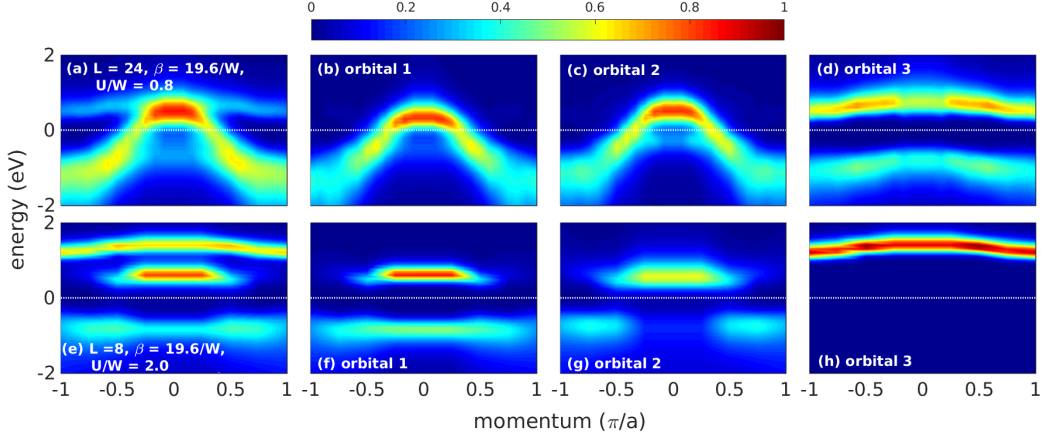


FIG. 6: (color online) (a) The spectral function for  $U/W = 0.8$ . (b), (c), and (d) are the orbital 1, 2, and 3 parts of the spectral function in (a), respectively. (e) The spectral function for  $U/W = 2$ . (f), (g), and (h) are the orbital 1, 2, and 3 parts of the spectral function in (e), respectively. The dash white line labels the Fermi surface. The inverse temperature is set as  $\beta = 19.6/W$ . Results were obtained with Maximum Entropy DQMC.

uation at hand, and thus the remaining nominally itinerant orbitals are decoupled from the localized orbital by the large  $J = U/4$ . This results in an effective nearly-degenerate two-band system with (nearly) three-quarters filling. This is special case for the two-orbital Hubbard model, which is prone to orbital ordering in one and two-dimensions.<sup>28,63,64</sup>

The situation is sketched in Fig. 7. Assuming ferromagnetic nearest neighbor correlations for orbital three, we have a low-energy ground state configuration as shown in the left side of 7a. Here, orbitals one and two adopt alternating double occupations in order to maximize their delocalization energy through virtual hopping processes. This results in near-neighbor orbital correlations. Subsequent charge fluctuations such as the one shown in the right side of the Fig. 7a cost a potential energy  $PE \sim U' - J = W/2$ . This is compensated for by a kinetic energy gain  $KE \sim 4t_{11} \sim 4W/4.9$ . The ratio between these competing energy scales is  $\sim 5/8$ , suggesting that charge fluctuations are strongly suppressed by the strong electronic correlations in this subsystem. Note that the situation is worse for antiferromagnetic nearest neighbor correlations in orbital three. The energy cost in this case increases to  $\sim U'$ , as shown in Fig. 7b. Thus both ferro- and antiferromagnetic correlations in orbital three will suppress charge fluctuations and promote orbital ordering. Since the type of magnetic correlations does not matter, such orbital ordering tendencies can be expected in the paramagnetic phases, provided the localized moments have formed in orbital three. This picture is then consistent with insulating behavior (and short-range orbital ordering tendencies, see below) at high temperatures, where no magnetic correlations are observed.

We verify this picture explicitly in Fig. 8, which plots the equal-time orbital correlation function  $\langle \hat{\tau}_{i+d} \hat{\tau}_i \rangle$ , with  $\hat{\tau}_i = (\hat{n}_{i,2} - \hat{n}_{i,1})$ . Here, results are shown for finite temperature DQMC calculations (Fig. 8a) and zero temper-

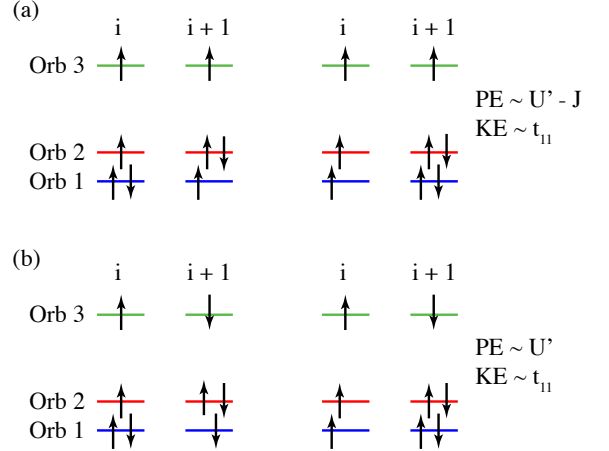


FIG. 7: A cartoon sketch of the relevant charge fluctuation processes leading to the insulating state when  $U/W = 2$  assuming (a) ferromagnetic and (b) antiferromagnetic nearest neighbor correlations within the orbital that has undergone the orbital selective Mott transition (orbital three).

ature DMRG calculations (Fig. 8b) and with  $U/W = 2$  in both cases. The “long-range” (with respect to the cluster size) anti-ferro-orbital correlation is clear in the zero temperature results obtained on  $L = 8$  and  $L = 16$  chains. At finite temperatures ( $\beta = 19.6/W$ ) we find that the orbital correlations are suppressed at long distances, but local anti-ferro-orbital correlation remains on shorter length scales. These combined results demonstrate the presence of short-range orbital correlations at higher temperatures, which grow in length as the temperature is decreased. The corresponding orbitally resolved DOS are plotted in Fig. 9 for both cases. Both methods predict that the system is insulating, with a charge gap width on orbitals one and two of about 0.5 eV. The



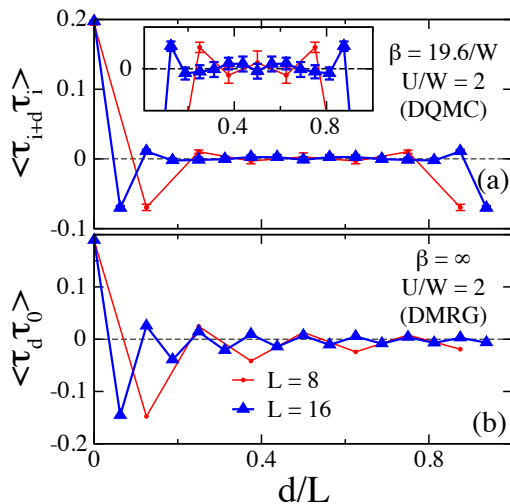


FIG. 8: Results for the orbital correlation function for the system in the strong coupling case  $U/W = 2$ . Results are obtained at (a) finite temperature using DQMC and (b)  $T = 0$  ( $\beta = \infty$ ) using DMRG. In both cases, results are shown on  $L = 8$  (red dots) and  $L = 16$  (blue triangles) chains. The DQMC results were obtained on a chain with periodic boundary conditions. The DMRG results were obtained on a chain with open boundary conditions.

presence of a gap at finite temperature also confirms that the short range orbital correlations are sufficient to open a gap in the spectral function. Finally, we stress these results will survive in the thermodynamic limit  $L \rightarrow \infty$ . This is confirmed in the inset in Fig. 9b, which shows the evolution of the  $T = 0$  gap  $\Delta$  as a function of  $L$ , as obtained from DMRG. Here, the gap size decreases with increasing chain lengths, however, it saturates to 0.2 eV for an infinite length chain.

#### IV. DISCUSSION AND SUMMARY

We have performed a momentum-resolved study of a multi-orbital model defined on extended 1D chains using non-perturbative DQMC and DMRG. This has allowed us to compute the several properties of an OSMP in a momentum resolved manner without resorting to approximate methods. We find that several properties do indeed exhibit significant momentum dependencies, not be captured by local approximations introduced by DMFT; however, the 1D case we have considered represents the worst case for DMFT. In that sense our results complement existing DMFT efforts by providing analysis in a region where the method is expected to perform badly.

Our results establish the hierarchy of charge and magnetic orderings in this model. At low temperatures, our DMRG calculations (as well as those in Ref. 37) demonstrate that orbital three is ferromagnetically ordered at  $T = 0$ . Contrary to this, our finite temperature DQMC

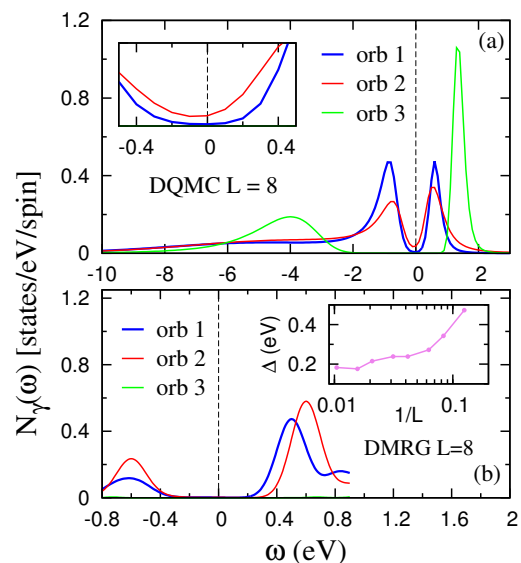


FIG. 9: Results for the orbitally-resolved density of states for each orbital obtained for  $U/W = 2$  and on  $L = 8$  site chains. Panel (a) shows DQMC results at  $\beta = 19.6/W$  and the inset zooms in to energy around Fermi surface. Panel (b) shows DMRG results for the same conditions but at zero temperature ( $\beta = \infty$ ). The inset plots a finite size scaling analysis of the charge gap obtained within DMRG (see text). The dash line in both panels indicates the Fermi energy.

calculations find no indications of any magnetic order for  $\beta < 19.6/W$ ; the magnetic structure factor  $S(q)$  is completely featureless as a function of  $q$  at these temperatures. Despite this, our finite  $T$  calculations find an orbital-selective Mott phase, as well as a fully insulating phase arising due to short-range orbital ordering, depending on the strength of the Hubbard interaction  $U$ . We therefore conclude that the charge ordering occurs before any magnetic ordering in this model.

The results shown in Fig. 2d and 3d show that orbital three in our model, which has the narrowest band width, undergoes a transition to a Mott phase at  $\beta W \sim 10 - 15$ . This in combination with the lack of magnetic signal means that OSMP in this parameter regime is a true Mott phase as opposed to a Slater insulator where the insulating behavior is driven by magnetism. Our results also demonstrate that it is insufficient to identify an OSMP using the orbital occupations only in some instances. One should be particularly careful in regions of parameter space where the itinerant bands have average occupations close to special cases known for one and two-orbital Hubbard models. In our case, the average fillings of the itinerant orbitals are  $\langle n_1 \rangle \sim 1.53$  and  $\langle n_2 \rangle \sim 1.47$ , values very close to the special case of  $3/4$  filling in a degenerate two-band Hubbard model. At zero temperature, our DMRG results obtain fillings of 1.5 for each orbital.

Finally, we discuss our results in the context of recent experimental work. ARPES results for  $\text{AFe}_2\text{As}_2$  have

found evidence that the OSMP in these materials disappears as the temperature is lowered.<sup>65</sup> This behavior was explained using a slave-boson approach and attributed to an increase in entropy associated with the OSMP. Our results do not show this behavior, and the OSMP is found at low temperature as one might naively expect. This difference may be related to the differences in the dimensionality (one vs. two) or number of orbitals (three vs. five) between the models or the differences between our non-perturbative approach and other mean-field methods. However, one would expect the entropy to be more important in one dimension. This highlights the need for continued application of non-perturbative methods to tractable multi-orbital Hubbard models.

*Acknowledgements* — The authors thank G. Liu for useful discussions. S. L., Y. W., and S. J. are supported by the University of Tennessee's Science Alliance Joint

Directed Research and Development (JDRD) program, a collaboration with Oak Ridge National Laboratory. N. K. and E. D. were supported by the National Science Foundation (NSF) under Grant No. DMR-1404375. Y. T. and T. A. M. acknowledge support by the Laboratory Directed Research and Development Program of Oak Ridge National Laboratory, managed by UT-Battelle, LLC, for the U.S. Department of Energy. Part of this work was conducted at the Center for Nanophase Materials Sciences, sponsored by the Scientific User Facilities Division (SUFD), BES, DOE, under contract with UT-Battelle. A.N. and G.A. acknowledge support by the Early Career Research program, SUFD, BES, DOE. CPU time was provided in part by resources supported by the University of Tennessee and Oak Ridge National Laboratory Joint Institute for Computational Sciences (<http://www.jics.utk.edu>).

- 
- <sup>1</sup> D. C. Johnston, *The Puzzle of High Temperature Superconductivity in Layered Iron Pnictides and Chalcogenides*. *Advances in Physics* **59**, 803 (2010).
  - <sup>2</sup> G. R. Stewart, *Superconductivity in iron compounds*. *Rev. Mod. Phys.* **83**, 1589 (2011).
  - <sup>3</sup> P. C. Dai, J. P. Hu, and E. Dagotto, *Magnetism and its microscopic origin in iron-based high-temperature superconductors*. *Nature Phys.* **8**, 709 (2012).
  - <sup>4</sup> A. van Roekeghem, P. Richard, H. Ding, S. Biermann, *Spectral properties of transition metal pnictides and chalcogenides: angle-resolved photoemission spectroscopy and dynamical mean field theory*. *C. R. Phys.* **17**, 140 (2016).
  - <sup>5</sup> R. Yu and Q. Si, *Orbital-Selective Mott Phase in Multi-orbital Models for Alkaline Iron Selenides  $K_{1-x}Fe_{2-y}Se_2$* . *Phys. Rev. Lett.* **110**, 146402 (2013).
  - <sup>6</sup> L. Fanfarillo and E. Bascones, *Electronic correlations in Hund metals*. *Phys. Rev. B* **92**, 075136 (2015).
  - <sup>7</sup> Y.-Z. Zhang, H. Lee, H.-Q. Lin, C.-Q. Wu, H. O. Jeschke, and R. Valentí, *General mechanism for orbital selective phase transitions*. *Phys. Rev. B* **85**, 035123 (2012).
  - <sup>8</sup> C. Knecht, N. Blümer, and P. G. J. van Dongen, *Orbital-selective Mott transitions in the anisotropic two-band Hubbard model at finite temperatures*. *Phys. Rev. B* **72**, 081103(R) (2005).
  - <sup>9</sup> A. Liebsch, *Novel Mott Transitions in a Nonisotropic Two-Band Hubbard Model*. *Phys. Rev. Lett.* **95**, 116402 (2005).
  - <sup>10</sup> A. Georges, L. de' Medici, and J. Mravlje, *Strong Correlations from Hund's Coupling*. *Annual Reviews of Condensed Matter Physics* **4**, 137 (2013).
  - <sup>11</sup> M. Ferrero, F. Becca, M. Fabrizio, and M. Capone, *Dynamical behavior across the Mott transition of two bands with different bandwidths*. *Phys. Rev. B* **72**, 205126 (2005).
  - <sup>12</sup> L. de' Medici, A. Georges, and S. Biermann, *Orbital-selective Mott transition in multiband systems: Slave-spin representation and dynamical mean-field theory*. *Phys. Rev. B* **72**, 205124 (2005).
  - <sup>13</sup> L. de' Medici, S. R. Hassan, M. Capone, and X. Dai, *Orbital-Selective Mott Transition out of band degeneracy lifting*. *Phys. Rev. Lett.* **102**, 126401 (2009).
  - <sup>14</sup> P. Werner and A. J. Millis, *High-Spin to Low-Spin and Orbital Polarization Transitions in Multiorbital Mott Systems*. *Phys. Rev. Lett.* **99**, 126405 (2007).
  - <sup>15</sup> A. Mukherjee, N. D. Patel, A. Moreo, and E. Dagotto, *Orbital selective directional conductor in the two-orbital Hubbard model*. *Phys. Rev. B* **93**, 085144 (2016).
  - <sup>16</sup> P. Sémon, K. Haule, and G. Kotliar, *Validity of the local approximation in iron-pnictides and chalcogenides*. *arXiv:1606.03660* (2016).
  - <sup>17</sup> N. Lanatà, H. U. R. Strand, G. Giovannetti, B. Hellsing, L. de' Medici, and M. Capone, *Orbital selectivity in Hund's metals: The iron chalcogenides*. *Phys. Rev. B* **87**, 045122 (2013).
  - <sup>18</sup> Z. P. Yin, K. Haule, and G. Kotliar, *Kinetic frustration and the nature of the magnetic and paramagnetic states in iron pnictides and iron chalcogenides*. *Nature Mat.* **10**, 932 (2011).
  - <sup>19</sup> V. I. Anisimov, I. A. Nekrasov, D. E. Kondakov, T. M. Rice, and M. Sigrist, *Orbital-selective Mott-insulator transition in  $Ca_{2-x}Sr_xRuO_4$* . *Eur. Phys. J. B* **25**, 191 (2002).
  - <sup>20</sup> N. Mannella, *The magnetic moment enigma in Fe-based high temperature superconductors*. *J. Phys.: Condens. Matter* **26** 473202 (2014).
  - <sup>21</sup> L. de' Medici, G. Giovannetti, and M. Capone, *Selective Mott Physics as a Key to Iron Superconductors*. *Phys. Rev. Lett.* **112**, 177001 (2014).
  - <sup>22</sup> For a recent review of DMFT, see Ref. 23. For a recent review of the application of DMFT to the electronic structure of the pnictides, see Ref.<sup>4</sup>
  - <sup>23</sup> A. Georges, G. Kotliar, W. Krauth, and M. J. Rozenberg, *Dynamical mean-field theory of strongly correlated fermion systems and the limit of infinite dimensions*. *Rev. Mod. Phys.* **68**, 13 (1996).
  - <sup>24</sup> A. Liebsch, *Single Mott transition in the multiorbital Hubbard model*. *Phys. Rev. B* **70**, 165103 (2004).
  - <sup>25</sup> S. Biermann, L. de' Medici, and A. Georges, *Non-Fermi-Liquid Behavior and Double-Exchange Physics in Orbital-Selective Mott Systems*. *Phys. Rev. Lett.* **95**, 206401 (2005).
  - <sup>26</sup> H. Ishida and A. Liebsch, *Fermi-liquid, non-Fermi-liquid, and Mott phases in iron pnictides and cuprates*. *Phys. Rev. B* **81**, 054513 (2010).
  - <sup>27</sup> M. Greger, M. Kollar, and D. Vollhardt, *Emergence of a*

- Common Energy Scale Close to the Orbital-Selective Mott Transition*. Phys. Rev. Lett. **110**, 046403 (2013).
- <sup>28</sup> C.-K. Chan, P. Werner, and A. J. Millis, *Magnetism and orbital ordering in an interacting three-band model: A dynamical mean-field study*. Phys. Rev. B **80**, 235114 (2009).
  - <sup>29</sup> H. Park, K. Haule, and G. Kotliar, *Cluster Dynamical Mean Field Theory of the Mott Transition*. Phys. Rev. Lett. **101**, 186403 (2008).
  - <sup>30</sup> E. Gull, P. Werner, X. Wang, M. Troyer, and A. J. Millis, *Local order and the gapped phase of the Hubbard model: A plaquette dynamical mean-field investigation*. Europhys. Lett. **84**, 37009 (2008).
  - <sup>31</sup> H. Lee, Y.-Z. Zhang, H. O. Jeschke, and R. Valentí, *Orbital-selective phase transition induced by different magnetic states: A dynamical cluster approximation study*. Phys. Rev. B **84**, 020401(R) (2011).
  - <sup>32</sup> H. Lee, Y.-Z. Zhang, H. O. Jeschke, R. Valentí, and H. Monien, *Dynamical Cluster Approximation Study of the Anisotropic Two-Orbital Hubbard Model*. Phys. Rev. Lett. **104**, 026402 (2010).
  - <sup>33</sup> K. S. D. Beach and F. F. Assaad, *Orbital-selective Mott transition and heavy-fermion behavior in a bilayer Hubbard model for  $^3\text{He}$* . Phys. Rev. B **83**, 045103 (2011).
  - <sup>34</sup> L. De Leo, M. Civelli, and G. Kotliar,  *$T = 0$  Heavy-Fermion Quantum Critical Point as an Orbital-Selective Mott Transition*. Phys. Rev. Lett. **101**, 256404 (2008).
  - <sup>35</sup> Y. Nomura, S. Sakai, and R. Arita, *Nonlocal correlations induced by Hund's coupling: A cluster DMFT study*. Phys. Rev. B **91**, 235107 (2015).
  - <sup>36</sup> K. Bouadim, G. G. Batrouni, and R. T. Scalettar, *Determinant Quantum Monte Carlo Study of the orbitally Selective Mott Transition*. Phys. Rev. Lett. **102**, 226402 (2009).
  - <sup>37</sup> J. Rincón, A. Moreo, G. Alvarez, and E. Dagotto, *Exotic Magnetic Order in the Orbital-Selective Mott Regime of Multiorbital Systems*. Phys. Rev. Lett. **112**, 106405 (2014).
  - <sup>38</sup> J. Rincón, A. Moreo, G. Alvarez, and E. Dagotto, *Quantum phase transition between orbital-selective Mott states in Hund's metals*. Phys. Rev. B **90**, 241105(R) (2014).
  - <sup>39</sup> G. Liu, N. Kaushal, S. Li, C. B. Bishop, Y. Wang, S. Johnston, G. Alvarez, A. Moreo, and E. Dagotto, *Study of the Orbital-Selective Mott Phases of a One-Dimensional Three-Orbital Hubbard Model Using Computational Techniques*. Phys. Rev. E **93**, 063313 (2016).
  - <sup>40</sup> J. M. Caron, J. R. Neilson, D. C. Miller, A. Llobet, and T. M. McQueen, *Iron displacements and magnetoelastic coupling in the antiferromagnetic spin-ladder compound  $\text{BaFe}_2\text{Se}_3$* . Phys. Rev. B **84**, 180409(R) (2011).
  - <sup>41</sup> J. M. Caron, J. R. Neilson, D. C. Miller, K. Arpino, A. Llobet, and T. M. McQueen, *Orbital-selective magnetism in the spin-ladder iron selenides  $\text{Ba}_{1-x}\text{K}_x\text{Fe}_2\text{Se}_3$* . Phys. Rev. B **85**, 180405(R) (2012).
  - <sup>42</sup> N. D. Patel, A. Nocera, G. Alvarez, R. Arita, A. Moreo, E. Dagotto, *Magnetic properties and pairing tendencies of the iron-based superconducting ladder  $\text{BaFe}_2\text{S}_3$ : combined ab initio and density matrix renormalization group study*. arXiv:1604.03621 (2016). To appear in Phys. Rev. B.
  - <sup>43</sup> S. Dong, J.-M. Liu, and E. Dagotto,  *$\text{BaFe}_2\text{Se}_3$ : A High  $T_c$  Magnetic Multiferroic with Large Ferrielectric Polarization*. Phys. Rev. Lett. **113**, 187204 (2014).
  - <sup>44</sup> Q. Luo, A. Nicholson, J. Rincón, S. Liang, J. Riera, G. Alvarez, L. Wang, W. Ku, G. D. Samolyuk, A. Moreo, and E. Dagotto, *Magnetic states of the two-leg-ladder alkali metal iron selenides  $\text{AFe}_2\text{Se}_3$* . Phys. Rev. B **87**, 024404 (2013).
  - <sup>45</sup> Q. Luo, K. Foyevtsova, G. D. Samolyuk, F. Reboredo, and E. Dagotto, *Magnetic states of the five-orbital Hubbard model for one-dimensional iron-based superconductors*. Phys. Rev. B **90**, 035128 (2014).
  - <sup>46</sup> S. R. White, D. J. Scalapino, R. L. Sugar, E. Y. Loh, J. E. Gubernatis, and R. T. Scalettar, *Numerical study of the two-dimensional Hubbard Model*. Phys. Rev. B **40**, 506 (1989).
  - <sup>47</sup> C. C. Chang, S. Gogolenko, J. Perez, Z. Bai, and R. T. Scalettar, *Recent Advances in Determinant Quantum Monte Carlo*. Philosophical Magazine B (2013). DOI:10.1080/14786435.2013.845314.
  - <sup>48</sup> L. Rademaker, S. Johnston, J. Zaanen, and J. van den Brink, *Determinant quantum Monte Carlo study of exciton condensation in the bilayer Hubbard model*. Phys. Rev. B **88**, 235115 (2013).
  - <sup>49</sup> S. R. White, *Density matrix formulation for quantum renormalization groups*. Phys. Rev. Lett. **69**, 2863 (1992).
  - <sup>50</sup> S. R. White, *Density-matrix algorithms for quantum renormalization groups*. Phys. Rev. B **48**, 10345 (1993).
  - <sup>51</sup> E. Y. Loh, Jr., J. E. Gubernatis, R. T. Scalettar, S. R. White, D. J. Scalapino, and R. L. Sugar, *Sign problem in the numerical simulation of many-electron systems*. Phys. Rev. B **41**, 9301 (1990).
  - <sup>52</sup> V. I. Iglovikov, E. Khatami, and R. T. Scalettar, *Geometry Dependence of the Sign Problem*, Phys. Rev. B **92**, 045110 (2015).
  - <sup>53</sup> K. Bouadim, G. G. Batrouni, F. Hébert, and R. T. Scalettar, *Magnetic and transport properties of a coupled Hubbard bilayer with electron and hole doping*. Phys. Rev. B **77**, 144527 (2008).
  - <sup>54</sup> M. Jarrell and J. E. Gubernatis, *Bayesian Inference and the analytic continuation of imaginary-time quantum Monte Carlo data*. Physics Reports **269**, 133 (1996).
  - <sup>55</sup> S. Fuchs, T. Pruschke, and M. Jarrell, *Analytic continuation of quantum Monte Carlo data by stochastic analytical inference*. Phys. Rev. E **81**, 056701 (2010).
  - <sup>56</sup> T. D. Kühner and S. R. White, *Dynamical correlation functions using the density matrix renormalization group*. Physical Review B **60**, 335 (1999).
  - <sup>57</sup> A. Nocera and G. Alvarez, *Spectral Functions with DMRG Revisited: Correction-vector with the Krylov-space Approach*. arXiv:1607.03538 (2016).
  - <sup>58</sup> O. Akerlund, P. de Forcrand, A. Georges, and P. Werner, *Dynamical mean field approximation applied to quantum field theory*. Phys. Rev. D **88**, 125006 (2013).
  - <sup>59</sup> N. Trivedi and M. Randeria, *Deviations from fermi-liquid behavior above  $T_c$  in 2D short coherence length superconductors*, Phys. Rev. Lett. **75**, 312 (1995).
  - <sup>60</sup> Shun Chi, S. Johnston, G. Levy, S. Grothe, R. Szedlak, B. Ludbrook, Ruixing Liang, P. Dosanjh, S. A. Burke, A. Damascelli, D. A. Bonn, W. N. Hardy, and Y. Pennec, *Sign inversion in the superconducting order parameter of  $\text{LiFeAs}$  inferred from Bogoliubov quasiparticle interference*. Phys. Rev. B **89**, 104522 (2014).
  - <sup>61</sup> A. Lankau, K. Koepernik, S. Borisenko, V. Zabolotnyy, B. Büchner, J. van den Brink, and H. Eschrig, *Absence of surface states for  $\text{LiFeAs}$  investigated using density functional calculations*. Phys. Rev. B **82**, 184518 (2010).
  - <sup>62</sup> H. Eschrig and K. Koepernik, *Tight-binding models for the iron-based superconductors*. Phys. Rev. B **80**, 104503 (2009).
  - <sup>63</sup> H. Sakamoto, T. Momoi, and K. Kubo, *Ferromagnetism in the one-dimensional Hubbard model with orbital degen-*

- eracy: From low to high electron density*. Phys. Rev. B **65**, 224403 (2002).
- <sup>64</sup> K. Held and D. Vollhardt, *Microscopic conditions favoring itinerant ferromagnetism: Hund's rule coupling and orbital degeneracy*, Eur. Phys. J. B **5**, 473 (1998).
- <sup>65</sup> M. Yi, D. H. Lu, R. Yu, S. C. Riggs, J. H. Chu, B. Lv, Z. K. Liu, M. Lu, Y. T. Cui, M. Hashimoto, S. K. Mo, Z. Hussain, C. W. Chu, I. R. Fisher, Q. Si, and Z. X. Shen, *Observation of Temperature-Induced Crossover to an Orbital-Selective Mott Phase in  $A_x\text{Fe}_{2-y}\text{Se}_2$  ( $A = \text{K}, \text{Rb}$ ) Superconductors*. Phys. Rev. Lett. **110**, 067003 (2013).